Research Article | Vol. 31, No. 10 / 8 May 2023 / Optics Express 16423

Optics EXPRESS

Study on the radiation and self-absorption characteristics of plasma under various background gases

JUNXIAO WANG,[1,2] ZHENRONG LIU,[3] LIPING ZHU,[4] ZHEN SONG,[1,2] YAN ZHANG,[5] LEI ZHANG,[1,2,*] WANFEI ZHANG,[3] GANG WANG,[3] ZEFU YE,[6] ZHUJUN ZHU,[6] WANGBAO YIN,[1,2,7] AND SUOTANG JIA[1,2]

[1]*State Key Laboratory of Quantum Optics and Quantum Optics Devices, Institute of Laser Spectroscopy, Shanxi University, Taiyuan 030006, China*
[2]*Collaborative Innovation Center of Extreme Optics, Shanxi University, Taiyuan 030006, China*
[3]*Shanxi Xinhua Chemical Defense Equipment Research Institute Co., Ltd., Taiyuan 030003, China*
[4]*Information Center of China North Industries Group, Beijing 100089, China*
[5]*School of Optoelectronic Engineering, Xi'an Technological University, Xian 710021, China*
[6]*Shanxi Gemeng U.S.-China Clean Energy R&D Center Co., Ltd., Taiyuan 030032, China*
[7]*ywb65@sxu.edu.cn*
[*]*k1226@sxu.edu.cn*

Abstract: The self-absorption effect is a primary factor responsible for the decline in the precision of quantitative analysis techniques using plasma emission spectroscopy, such as laser-induced breakdown spectroscopy (LIBS). In this study, based on the thermal ablation and hydrodynamics models, the radiation characteristics and self-absorption of laser-induced plasmas under different background gases were theoretically simulated and experimentally verified to investigate ways of weakening the self-absorption effect in plasma. The results reveal that the plasma temperature and density increase with higher molecular weight and pressure of the background gas, leading to stronger species emission line intensity. To reduce the self-absorption effect in the later stages of plasma evolution, we can decrease the gas pressure or substitute the background gas with a lower molecular weight. As the excitation energy of the species increases, the impact of the background gas type on the spectral line intensity becomes more pronounced. Moreover, we accurately calculated the optically thin moments under various conditions using theoretical models, which are consistent with the experimental results. From the temporal evolution of the doublet intensity ratio of species, it is deduced that the optically thin moment appears later with higher molecular weight and pressure of the background gas and lower upper energy of the species. This theoretical research is essential in selecting the appropriate background gas type and pressure and doublets in self-absorption-free LIBS (SAF-LIBS) experiments to weaken the self-absorption effect.

1. Introduction

Laser-induced breakdown spectroscopy (LIBS) is an emerging technique for qualitative and quantitative analysis of substances based on plasma emission spectroscopy. Due to the advantages of simultaneous analysis of multiple elements, almost no damage to samples, and applicability to harsh environments, it has been widely used in cultural heritage [1–3], biomedicine [4–6], space exploration [7–9] and other fields. However, the inherent self-absorption effect in LIBS can reduce the accuracy of its quantitative analysis. This effect is caused by the non-uniformity of temperature in the plasma, where the temperature at the center is higher than that at the edge. When photons generated by spontaneous radiation of internal species in excited state at high

#489720 https://doi.org/10.1364/OE.489720
Journal © 2023 Received 10 Mar 2023; revised 17 Apr 2023; accepted 17 Apr 2023; published 1 May 2023

Optics EXPRESS

energy level propagate outward, they will be reabsorbed by similar species at low energy level in the transmission path, resulting in a reduction in the observed spectral line intensity.

In recent years, numerous studies have been conducted on the self-absorption effect in plasma. For example, Rezaei et al. theoretically investigated the self-absorption in early plasma in helium and argon, and found that the self-absorption effect in argon was more pronounced, and the self-absorption (SA) coefficient decreased with delay [10]. Based on the study of self-absorption under different atmospheric pressures, Hao et al. concluded that the plasma without self-absorption and calibration curve with high linear correlation could be obtained by reducing atmospheric pressure [11]. Hai et al. compared the self-absorption of plasma generated in air and argon under different laser fluences, and found that the argon environment and the increase of laser fluence both significantly reduced the self-absorption effect [12]. Tang et al. used the exponential calibration curve to evaluate the self-absorption under different delays and acquisition gate widths, and found that the calibration curve under the time window with minimum self-absorption had better linearity than the result under the traditional optimized time window [13]. Jabbar et al. studied the influence of gas pressure and laser energy on the intensity ratio, and provided the ranges of gas pressure and laser energy when the plasma is optically thin [14]. Building upon these previous studies, we have proposed the theory and method of self-absorption-free LIBS (SAF-LIBS), which involves determining the moment when the plasma is optically thin by comparing the intensity ratio of the doublet with similar upper energies with the theoretical value, capturing quasi-optically thin spectral lines [15]. We then used resonant and non-resonant doublets to establish calibration curves, enabling SAF-LIBS to have both a low detection limit and a wide detectable content range [16]. In addition, through theoretical analysis of the temporal evolution trend of doublet intensity ratio, we have proposed a rapid selection criterion of doublets for SAF-LIBS [17].

Building upon previous theoretical studies on the evolution of plasma parameters in SAF-LIBS under various inert gases and pressures [18], this paper presents a theoretical analysis of the radiation characteristics and self-absorption effect of plasma under various background gases, considering the self-absorption effect. This work will guide the optimization of experimental parameters and reduce the impact of the self-absorption effect on the quantitative analysis accuracy of LIBS.

2. Theoretical models

2.1. Heating of sample

When a laser is vertically incident on a sample, the sample temperature rises after absorbing the laser energy. This process can be described by the following heat conduction equation [19,20]:

$$c_p \rho_s \left(\frac{\partial T_s}{\partial t} - v \frac{\partial T_s}{\partial z} \right) = \lambda_s \frac{\partial^2 T_s}{\partial z^2} + (1 - R)\, \alpha I \exp(-\alpha z), \tag{1}$$

where c_p, ρ_s, λ_s, R and α are the specific heat, mass density, thermal conductivity, reflectivity and absorption coefficient of the sample respectively, T_s is the temperature of the sample, v is the evaporation rate, I is the laser power density reaching the sample surface after considering the shielding effect, and z is the coordinate along the inward normal to the sample.

2.2. Expansion of plasma

When the temperature of the laser heating area reaches the boiling point, vapor species are generated, which continue to absorb laser energy and further ionize to form vapor plasma. The

Optics EXPRESS

expansion process of plasma can be described by hydrodynamics equations [19,21]:

$$\frac{\partial \rho_i}{\partial t} + \nabla \cdot (\rho_i \boldsymbol{u}) = 0, \tag{2}$$

$$\frac{\partial \rho \boldsymbol{u}}{\partial t} + \nabla \cdot (\rho \boldsymbol{u} u) = \nabla \cdot \boldsymbol{\tau} - \nabla p, \tag{3}$$

$$\frac{\partial \rho \left(e + \frac{\boldsymbol{u}^2}{2}\right)}{\partial t} + \nabla \cdot \left(\rho \left(e + \frac{\boldsymbol{u}^2}{2}\right) \boldsymbol{u}\right) = \nabla \cdot (\boldsymbol{\tau} \cdot \boldsymbol{u}) - \nabla \cdot (p\boldsymbol{u}) - \nabla \cdot \boldsymbol{q} - q^{rad} + (\alpha_{IB} + \alpha_{PI})\, I, \tag{4}$$

where ρ_i, ρ, $\boldsymbol{u}$, p, e and q^{rad} are the mass density of species i, total mass density, expansion velocity, local pressure, specific internal energy, and power loss, respectively, $\boldsymbol{\tau}$ and $\boldsymbol{q}$ are the viscous stress tensor and heat conduction flux, and α_{IB} and α_{PI} are the inverse bremsstrahlung absorption coefficient and photoionization coefficient.

2.3. Spectra of plasma

Under the condition of local thermal equilibrium, considering the influence of self-absorption effect, the emission intensity of spectral lines (u-l transition) in the plasma is:

$$I_i^{ul} = SA \frac{n_i g_u A_{ul}}{\lambda_{ul} U} \exp(-\frac{E_u}{k_B T_e}), \tag{5}$$

where n_i is the number density of species i, A_{ul} is the transition probability, λ_{ul} is the wavelength, g_u is the degeneracy, E_u is the energy of the upper energy level, k_B is the Boltzmann constant, U is the partition function, and T_e is the plasma temperature.

3. Results and discussion

Next, we studied the radiation characteristics and self-absorption effects of Mg and Al species according to the above model, and the spectral parameters used were given from the NIST database, as shown in Table 1.

Table 1. Spectral parameters of Mg and Al species obtained from the NIST database

Species	λ_{ul} (nm)	A_{ul} ($\times 10^7$ s^{-1})	g_u	E_u (eV)
Mg I	517.27	3.37	3	5.11
	518.36	5.61	3	5.11
Mg II	448.11	23.3	8	11.63
Al I	394.40	4.99	2	3.14
	396.15	9.85	2	3.14
Al II	358.66	23.5	9	15.30

3.1. Radiation characteristics of plasma

Figure 1(a) displays the normalized intensities of Al I and Mg I lines in the 350-550 nm band under various background gases at 2 μs delay, in which the illustrations represent local enlarged images of the spectral peaks. The spectral line intensity under air (average molecular weight = 29) is similar to that under nitrogen (molecular weight = 28) and oxygen (molecular weight = 32), while the line intensity under argon (molecular weight = 40) is the strongest, and that under nitrogen is relatively weak. According to the intensity evolution under various background gases, the spectral line intensity of species increases with the increase of molecular weight of the

Optics EXPRESS

background gas. Since the spectral line intensity is closely related to species number density and electron temperature, Fig. 1(b) shows the number density of Al I and Mg I species and electron temperature under each background gas, where red and orange spheres represent Al I and Mg I species, respectively. The species number density and electron temperature increase with the increase of the background gas density. In dense background gas, gas molecules limit the expansion of vapor plasma, which results in strong spectral line intensity for high-temperature and high-density plasma. This phenomenon was also observed in the experiment of laser ablation of copper in three background gases (He, Ne, and Ar), that is, the temperature and electron number density were higher for ablation in a gas with higher atomic mass [22]. Additionally, Fig. 1(a) shows that the signal enhancement of different species under high-density gas compared to low-density gas is also different, which will be further analyzed.

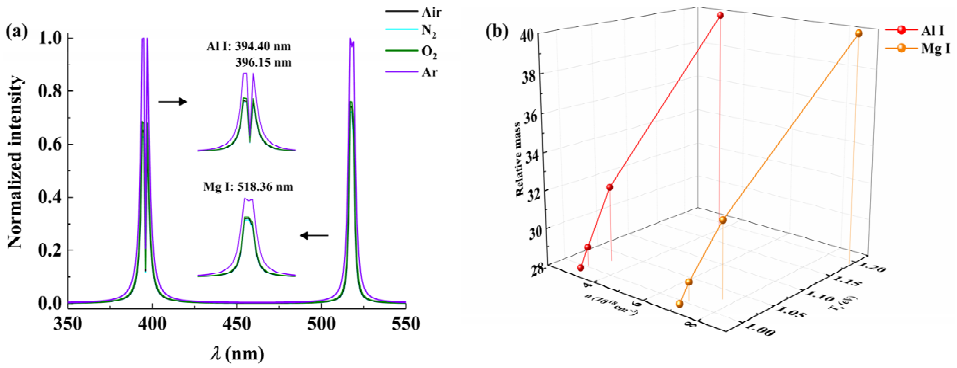

Fig. 1. (a) Normalized intensities of Al I and Mg I lines and (b) species number densities and electron temperatures at 2 μs delay under various background gases.

According to the emission intensity of the spectral lines in Eq. (5) and Saha equation, the intensity of the atomic and ionic lines can be expressed as:

$$I_I = SA_I \frac{hcB_I g_I N_0}{\lambda_I U_0} \exp\left(-\frac{E_I}{k_B T}\right), \tag{6}$$

$$I_{II} = SA_{II} \frac{hcB_{II} g_{II} N_0}{\lambda_{II} U_0} \frac{2(2\pi m_e k_B)^{3/2}}{h^3} \frac{T^{3/2}}{N_e} \exp\left(-\frac{E_{II} + E_{IP}}{k_B T}\right), \tag{7}$$

where E_{IP} is the ionization potential.

For species with the same transition, the intensity ratio in argon to air is:

$$\frac{I_{0I,Ar}}{I_{0I,Air}} = \frac{I_{I,Ar} SA_{I,Air}}{I_{I,Air} SA_{I,Ar}} = \frac{N_{0,Ar} U_{0,Air}}{N_{0,Air} U_{0,Ar}} \exp\left(-\frac{1}{k_B}\left(\frac{1}{T_{Ar}} - \frac{1}{T_{Air}}\right) \times E_I\right), \tag{8}$$

$$\frac{I_{0II,Ar}}{I_{0II,Air}} = \frac{I_{II,Ar} SA_{II,Air}}{I_{II,Air} SA_{II,Ar}} = \frac{N_{0,Ar} U_{0,Air}}{N_{0,Air} U_{0,Ar}} \frac{T_{Ar}^{3/2}}{T_{Air}^{3/2}} \frac{N_{e,Air}}{N_{e,Ar}} \exp\left(-\frac{1}{k_B}\left(\frac{1}{T_{Ar}} - \frac{1}{T_{Air}}\right) \times (E_{II} + E_{IP})\right). \tag{9}$$

Taking the 2 μs delay as an example, the plasma temperature under argon and air is 1.19 eV and 1.00 eV, and the electron number density is $2.50 \times 10^{16}\,\mathrm{cm}^{-3}$ and $1.81 \times 10^{16}\,\mathrm{cm}^{-3}$, respectively. The expression $(T_{Ar}/T_{Air})^{3/2} N_{e,Air}/N_{e,Ar}$ can be ignored since it is approximately equal to 1. Therefore, for atomic and ionic spectral lines, the intensity ratio in argon to air can be simplified as:

$$\frac{I_{0,Ar}}{I_{0,Air}} = A \exp(B \times E_k^*), \tag{10}$$

where $A = (N_{0,Ar} U_{0,Air})/(N_{0,Air} U_{0,Ar})$, $B = -(1/T_{Ar} - 1/T_{Air})/k_B$, for atoms, $E^* k = E_I$, and for ions $E^* k = E_{II} + E_{IP}$.

Optics EXPRESS

At 2 μs delay, the plasma temperature and electron number density under nitrogen are 0.99 eV and 1.78×10^{16} cm^{-3} respectively, which are similar to those under air. Thus, the expression $(T_{N2}/T_{Air})^{3/2} N_{e,Air}/N_{e,N2}$ can also be ignored, and the intensity ratio in nitrogen and air can be described by Eq. (10). Since the expression -($1/T_{N2}$ -$1/T_{Air}$)/k_B approaches 0, according to the Taylor expansion of the exponential function, it can be further simplified as:

$$\frac{I_{0,N_2}}{I_{0,Air}} = A\left(1 - \frac{1}{k_B}\left(\frac{1}{T_{N_2}} - \frac{1}{T_{Air}}\right) \times E_k^*\right). \tag{11}$$

Figure 2 shows the evolution of the intensity ratio in argon and nitrogen to air with the upper energy of different species at 2 μs delay, where the solid square represents the intensity ratio of theoretical simulation, and the solid line is the fitting curve. As seen in the figure, the exponential and linear functions can well fit the evolution trend of the intensity ratio in argon and nitrogen to air. The intensity ratio in argon to air increases with the increase of the species upper energy, whereas the intensity ratio in nitrogen to air decreases with the increase of the upper energy. Compared to the intensity under air, the corresponding spectral line intensity under other background gases changes more drastically with higher upper energy. In other words, the greater the increase of spectral line intensity under argon, the greater the decrease of spectral line intensity under nitrogen.

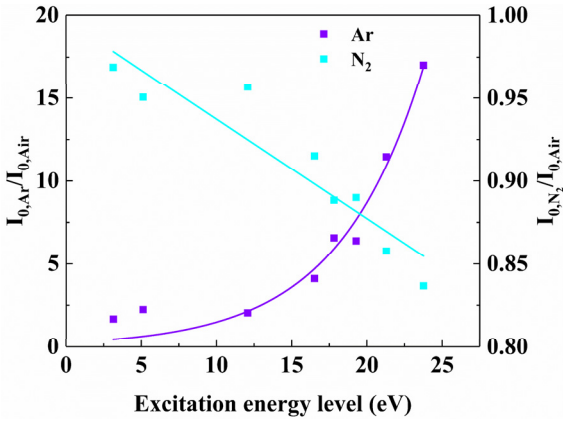

Fig. 2. Relationship between intensity ratio and species upper energy under various background gases at 2 μs delay.

In addition to investigating the influence of background gas type on the radiation properties, we also explored the effect of background gas pressure on species intensity in plasma. Figure 3 illustrates the temporal evolution of intensity ratio at 1000 mbar compared to other argon pressures within the 0.5-2.5 μs delay. As shown in the figure, the intensity ratio gradually increases at first and then decreases towards the end of plasma evolution. With the increase of argon pressure, the plasma temperature and species number density also increase, leading to the increase in spectral line intensity. Furthermore, the higher the excitation energy, the more pronounced the increase in intensity ratio.

3.2. SA coefficient

The SA coefficient provides a more intuitive measure of the self-absorption degree of spectral lines, which is closely related to factors such as the background gas and species, and can vary with experimental conditions. In the study of SA coefficient, for Al I and Mg I species, we choose a stronger line of the doublet, namely Al I 396.15 nm and Mg I 518.36 nm. Figure 4(a)

Optics EXPRESS

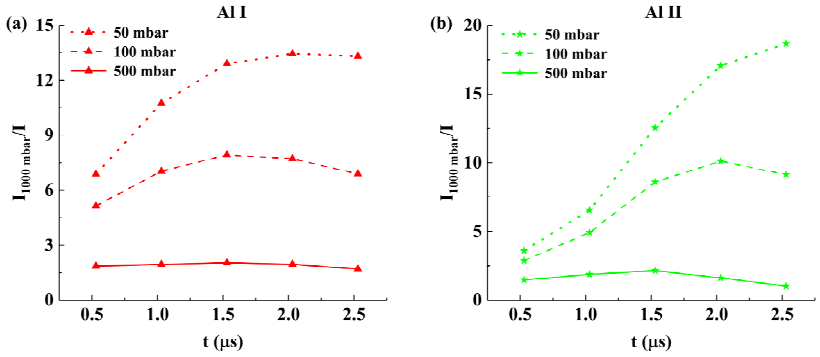

Fig. 3. Temporal evolution of intensity ratio of (a) Al I and (b) Al II species under various argon pressures.

illustrates the relationship between the SA coefficients of Al and Mg species emission spectral lines and the molecular weight of the background gas at a delay of 2 μs, with species represented by different colors. It is evident that, towards the end of the plasma evolution, the SA coefficients of all species show a negative correlation with the molecular weight of the background gases, indicating that as the molecular weight of the background gas increases, the self-absorption effect becomes more severe, leading to a decrease in the SA coefficient. This finding is consistent with the results presented in Fig. 1(a), which shows that the intensity of Mg I species at 518.36 nm under argon is significantly lower than in other gases. As the molecular weight of the background gas increases, the plasma temperature and species number density increase, resulting in a more pronounced self-absorption effect. Furthermore, a comparison of the four species reveals that lower energy species exhibit larger SA coefficient and smaller self-absorption degree. Species at the edge of the plasma have lower energy levels than those at the center, making photons emitted by lower-energy species at the center more readily absorbed by species at the edge. Figure 4(b) shows the relationship between the SA coefficients of Al I and Al II lines and the molecular weight of the background gas at 0.5 μs and 1 μs. It is evident that at the early stage of plasma expansion, the SA coefficient of Al I species increases with increasing molecular weight of the background gas, which is the opposite trend to that observed at 2 μs. Previous literature also suggests that the presence of an argon atmosphere reduces the self-absorption effect [12]. Moreover, the self-absorption effects of ionic lines are more pronounced than those of atomic lines at 0.5 μs.

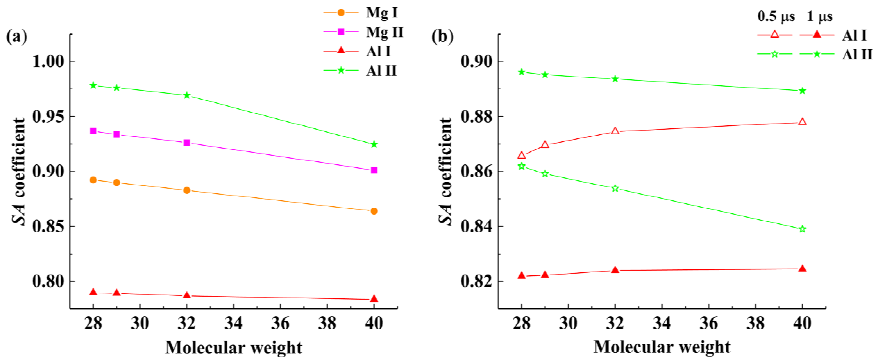

Fig. 4. Relationship between the SA coefficients of (a) Al and Mg species at 2 μs and (b) Al species at 0.5 μs and 1 μs and the molecular weight of the background gas.

Optics EXPRESS

Figure 5(a) depicts the relationship between the SA coefficients of Al and Mg species and the pressure of argon at 2 μs. It is evident that the self-absorption effects of ionic lines become more significant with increasing argon pressure, while the self-absorption effects of atomic lines become more significant with decreasing argon pressure. It is speculated that, for atoms, the reduction of pressure accelerates the diffusion of species at the center, resulting in a higher atomic number density at the edge of the plasma than at the center, thereby enhancing the self-absorption effect. Figure 5(b) illustrates the relationship between the SA coefficients of Al I and Al II species and the pressure at 0.5 μs and 1 μs. The figure clearly shows that at the early stage of plasma, the self-absorption effects of ionic lines are stronger than those of atomic lines.

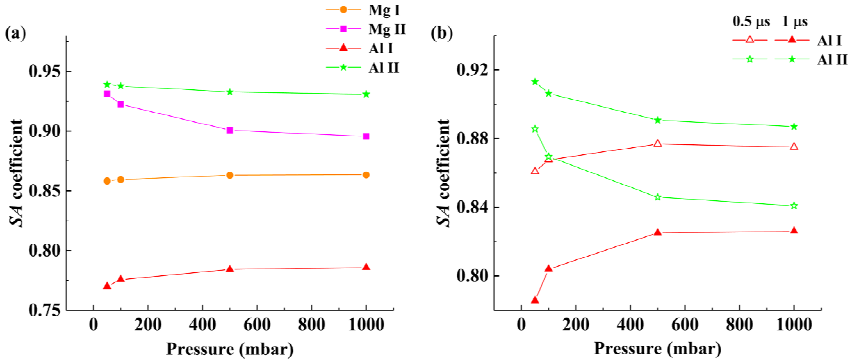

Fig. 5. Relationship between the SA coefficients of (a) Al and Mg species at 2 μs and (b) Al species at 0.5 μs and 1 μs and the pressure of argon.

3.3. *Optically thin moment*

The study of SA coefficients gives us a rough understanding of the evolution of self-absorption effect with molecular weight and pressure of the background gas under different species and delays. To accurately identify a plasma without self-absorption effect, we can calculate the optically thin moment by using SAF-LIBS.

Under the assumption of local thermal equilibrium, if the plasma is in the optically thin state, the doublet intensity ratio of the same element in the same ionization state can be expressed as [15,16]:

$$\frac{I_{0,1}}{I_{0,2}} = \frac{\lambda_{ul} A_{kj} g_k}{\lambda_{kj} A_{ul} g_u} \exp\left(-\frac{E_k - E_u}{k_B T}\right), \tag{12}$$

where $I_{0,1}$, $I_{0,2}$ are the spectral line intensities of transitions from the energy level k to j and u to l, respectively.

When the upper energies of the doublets are the same or close, the exponential term in the above equation is equal to or approximately equal to 1, so Eq. (12) can be simplified as:

$$\frac{I_{0,1}}{I_{0,2}} = \frac{\lambda_{ul} A_{kj} g_k}{\lambda_{kj} A_{ul} g_u}. \tag{13}$$

As can be seen, in the optically thin state, the doublet intensity ratio with similar upper energies is only dependent on spectroscopic parameters of the spectral lines and is a constant. Therefore, once the experimentally measured intensity ratio at a certain moment equals to the theoretical value, we can consider that there is no self-absorption effect, and that moment is the optically thin moment. In this way, by setting the exposure delay time to this moment, we can convert LIBS to SAF-LIBS.

Optics EXPRESS

Figure 6 shows the temporal evolution of doublet intensity ratio of Al I 396.15 nm and Al I 394.40 nm, Mg I 518.36 nm and Mg I 517.27 nm under air and argon obtained through theoretical simulation. According to the theory of self-absorption-free [15,16], the doublet intensity ratio of Al I species in the optically thin state is 1.97. Considering the self-absorption effect, the doublet intensity ratio of Al I species increases first and then decreases with the delay time, and the optically thin moments under air and argon are respectively 1.77 μs and 2.17 μs. Similarly, the doublet intensity ratio of Mg I species in Fig. 6(b) increases first and then decreases with the delay time, intersecting the theoretical level of 1.66 at 0.78 μs and 0.95 μs respectively under air and argon. It can be seen that the optically thin moment of Mg I doublet is much earlier than that of Al I doublet. The optically thin moments of different doublets are different, and the optically thin moment of atoms with higher energy occurs earlier than that of atoms with lower energy. This is consistent with the conclusion in [23] that the lower the upper energy, the longer the species lifetime, and the later the optically thin moment appears. Table 2 lists the optically thin moments of Al and Mg lines calculated under various background gases and pressures, showing that the larger the molecular weight of the background gas and the higher the pressure, the later the optically thin state of the plasma appears.

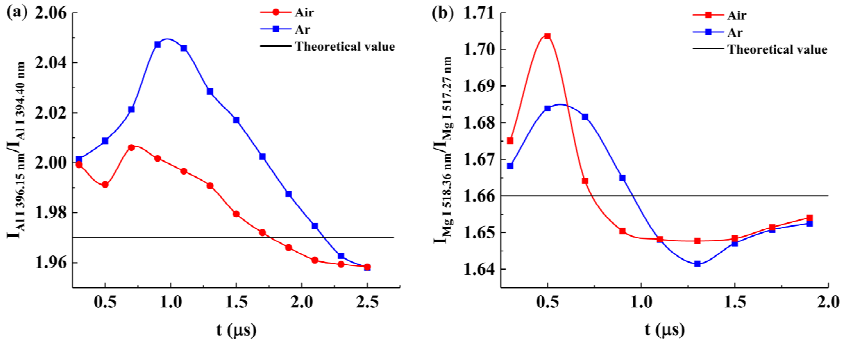

Fig. 6. Temporal evolution and theoretical values of doublet intensity ratios of (a) Al I and (b) Mg I species under air and argon.

Table 2. Optically thin moments of Al and Mg lines under various background gases at one atmosphere and argon pressures

Background gas	Nitrogen	Air	Oxygen	Argon
$t_{Al\ I}$ (μs)	1.757	1.774	2.039	2.168
$t_{Mg\ I}$ (μs)	0.745	0.779	0.820	0.949
Pressure (mbar)	50	100	500	1000
$t_{Al\ I}$ (μs)	0.570	0.830	1.567	2.168
$t_{Mg\ I}$ (μs)	0.465	0.620	0.879	0.949

3.4. *Verification of optically thin moment*

In the experiment, an Al-Mg alloy with a mass ratio of 49:1 was used as the sample. A Nd: YAG laser (Spectra Physics, INDI-HG-20S) output 1064 nm, 100 mJ/pulse laser pulses with a repetition rate of 10 Hz and was focused 7 mm below the sample surface to generate plasmas. The fluorescence was collected by an optical fiber and transmitted to a diffraction grating spectrometer (Princeton Instruments, SP-2750), and the spectra were detected by an ICCD (Princeton Instruments, PI-MAX4-1024i). The sample was placed on a three-dimensional

Optics EXPRESS

translation platform, and each point was hit with 3 laser pulses before being replaced with a fresh point. Each group of spectral data was the average of 60 spectra obtained by laser ablation of 20 points on the sample surface.

Figure 7 shows the temporal evolution of the doublet intensity ratios of Al I and Mg I doublets obtained experimentally under air and argon. In the studied time domain, the intensity ratios of these doublets both exhibit an overall monotonic downward trend with time. The intersection in the figure represents the experimentally obtained intensity ratio that equals the theoretical value, indicating that the spectral lines are at an optically thin moment with no self-absorption effect present. It can be seen from the figure that under air and argon, the optically thin moments of Al I doublet are 1.13 μs and 1.24 μs respectively, while those of Mg I doublet are 0.76 μs and 0.93 μs respectively. The argon atmosphere prolonged the appearance of the optically thin state, and the optically thin moment of the Mg I doublet was earlier than that of the Al I doublet, which is consistent with the above simulation results, thus confirming the reliability of our theoretical method. In addition, it can also be seen from Figs. 6 and 7 that the experimentally measured doublet intensity ratio is larger and the optically thin moment is earlier compared to the theoretical simulation results. This may be attributed to factors such as sample heterogeneity, integration time, fiber alignment angle, etc. For example, the integration time in the theoretical simulation was 1 ns, while in the experiment it was set to 500 ns.

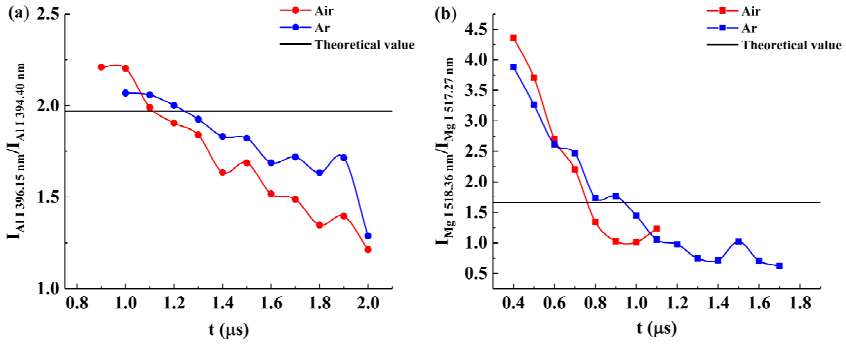

Fig. 7. Temporal evolution of doublet intensity ratios of (a) Al I and (b) Mg I lines under air and argon.

4. Conclusion

In this work, based on the thermal ablation and hydrodynamics models, the radiation characteristics and self-absorption effects of laser-induced plasma under various background gases were studied. The increase in molecular weight of the background gas leads to the generation of a higher temperature and density plasma, thus increasing the emission intensity of spectral lines. Compared to air, the molecular weight of the background gas has a more significant effect on the species in the high excitation energy level. The increase in background gas pressure also leads to an increase in spectral line intensity, and the increase of ionic lines is greater than that of atomic lines. By studying the SA coefficients of species under different delays, it was found that the self-absorption effects of ionic lines are larger than those of atomic lines in the early stage of plasma evolution. Additionally, the moment when the plasma is in the optically thin state was found by using the intensity ratio of doublets with similar upper energies. It was found that the greater the molecular weight and pressure of the background gas and the lower the upper energy of species, the later the optically thin moment appears. The simulation results were well verified by experiments. This work is of great significance for the selection of the type and pressure

Optics EXPRESS

of background gas, the rapid selection of suitable doublet, the determination of optically thin moment and the improvement of measurement accuracy in SAF-LIBS experiments.

Funding. National Key Research and Development Program of China (2017YFA0304203); National Energy R&D Center of Petroleum Refining Technology; Changjiang Scholars and Innovative Research Team in University of Ministry of Education of China (IRT_17R70); National Natural Science Foundation of China (61975103, 627010407); 111 Project (D18001); Fund for Shanxi "1331KSC".

Disclosures. The authors declare no conflicts of interest.

Data availability. Data underlying the results presented in this paper are not publicly available at this time but may be obtained from the authors upon reasonable request.

References

1. R. Gaudiuso, M. Dell'Aglio, O. D. Pascale, G. S. Senesi, and A. D. Giacomo, "Laser Induced Breakdown Spectroscopy for Elemental Analysis in Environmental, Cultural Heritage and Space Applications: A Review of Methods and Results," Sensors **10**(8), 7434–7468 (2010).
2. A. Botto, B. Campanella, S. Legnaioli, M. Lezzerini, G. Lorenzetti, S. Pagnotta, F. Poggialini, and V. Palleschi, "Applications of laser-induced breakdown spectroscopy in cultural heritage and archaeology: a critical review," J. Anal. At. Spectrom. **34**(1), 81–103 (2019).
3. V. Detalle and X. S. Bai, "The assets of laser-induced breakdown spectroscopy (LIBS) for the future of heritage science," Spectrochim. Acta, Part B **191**, 106407 (2022).
4. X. Y. Liu and W. J. Zhang, "Recent developments in biomedicine fields for laser induced breakdown spectroscopy," J. Biomedical Science and Engineering **01**(03), 147–151 (2008).
5. V. K. Singh, J. Sharma, A. K. Pathak, C. T. Ghany, and M. A. Gondal, "Laser-induced breakdown spectroscopy (LIBS): a novel technology for identifying microbes causing infectious diseases," Biophys. Rev. **10**(5), 1221–1239 (2018).
6. T. C. Zanetti, T. A. Catelani, E. R. Pereira-Filho, and J. S. Cabral, "Laser-induced breakdown spectroscopy as a tool for homogeneity measurements in medicine tablets," Laser Phys. **30**(3), 035701 (2020).
7. A. K. Knight, N. L. Scherbarth, D. A. Cremers, and M. J. Ferris, "Characterization of Laser-Induced Breakdown Spectroscopy (LIBS) for Application to Space Exploration," Appl. Spectrosc. **54**(3), 331–340 (2000).
8. S. G. Pavlov, E. K. Jessberger, H. W. Hübers, S. Schröder, I. Rauschenbach, S. Florek, J. Neumann, H. Henkel, and S. Klinkner, "Miniaturized laser-induced plasma spectrometry for planetary in situ analysis – The case for Jupiter's moon Europa," Adv. Space Res. **48**(4), 764–778 (2011).
9. C. Q. Liu, Z. C. Ling, J. Zhang, Z. C. Wu, H. C. Bai, and Y. H. Liu, "A Stand-Off Laser-Induced Breakdown Spectroscopy (LIBS) System Applicable for Martian Rocks Studies," Remote Sens. **13**(23), 4773 (2021).
10. F. Rezaei, P. Karimi, and S. H. Tavassoli, "Estimation of self-absorption effect on aluminum emission in the presence of different noble gases: comparison between thin and thick plasma emission," Appl. Opt. **52**(21), 5088–5096 (2013).
11. Z. Q. Hao, L. Liu, M. Shen, X. Y. Yang, K. H. Li, L. B. Guo, X. Y. Li, Y. F. Lu, and X. Y. Zeng, "Investigation on self-absorption at reduced air pressure in quantitative analysis using laser-induced breakdown spectroscopy," Opt. Express **24**(23), 26521–26528 (2016).
12. R. Hai, Z. L. He, X. Yu, L. Y. Sun, D. Wu, and H. B. Ding, "Comparative study on self-absorption of laser-induced tungsten plasma in air and in argon," Opt. Express **27**(3), 2509–2520 (2019).
13. Y. Tang, S. X. Ma, Y. W. Chu, T. Wu, Y. Y. Ma, Z. L. Hu, L. B. Guo, X. Y. Zeng, J. Duan, and Y. F. Lu, "Investigation of the self-absorption effect using time-resolved laser-induced breakdown spectroscopy," Opt. Express **27**(4), 4261–4270 (2019).
14. A. Jabbar, M. Akhtar, J. Iqbal, S. Mahmood, and M. A. Baig, "Spectroscopic investigation of laser-produced strontium plasma using fundamental and second harmonics of Nd: YAG laser," IEEE Trans. Plasma Sci. **49**(5), 1564–1573 (2021).
15. J. J. Hou, L. Zhang, W. B. Yin, S. C. Yao, Y. Zhao, W. G. Ma, L. Dong, L. T. Xiao, and S. T. Jia, "Development and performance evaluation of self-absorption-free laser-induced breakdown spectroscopy for directly capturing optically thin spectral line and realizing accurate chemical composition measurements," Opt. Express **25**(19), 23024–23034 (2017).
16. J. J. Hou, L. Zhang, Y. Zhao, W. G. Ma, L. Dong, W. B. Yin, L. T. Xiao, and S. T. Jia, "Resonance/non-resonance doublet-based self-absorption-free LIBS for quantitative analysis with a wide measurement range," Opt. Express **27**(3), 3409–3421 (2019).
17. J. J. Hou, L. Zhang, Y. Zhao, W. G. Ma, L. Dong, W. B. Yin, L. T. Xiao, and S. T. Jia, "Rapid selection of analytical lines for SAF-LIBS based on the doublet intensity ratios at the initial and final stages of plasma," Opt. Express **27**(22), 32184–32192 (2019).
18. J. X. Wang, L. Zhang, S. Q. Wang, M. G. Su, D. X. Sun, J. H. Han, G. F. Xia, C. Z. Dong, Q. Min, W. G. Ma, L. Dong, W. B. Yin, L. T. Xiao, and S. T. Jia, "Numerical simulation of laser-induced plasma in background gas considering multiple interaction processes," Plasma Sci. Technol. **23**(3), 035001 (2021).
19. D. Bhattacharya, R. K. Singh, and P. H. Holloway, "Laser-Target Interactions During Pulsed Laser Deposition of Superconducting Thin Films," J. Appl. Phys. (Melville, NY, U. S.) **70**(10), 5433–5439 (1991).

Optics EXPRESS

20. J. X. Wang, Y. Zhao, L. Zhang, S. Q. Wang, M. G. Su, D. X. Sun, Q. Min, W. G. Ma, W. B. Yin, and S. T. Jia, "Kinetic Evolution of Laser Ablating Alloy Materials," Front. Phys. **9**, 812283 (2021).
21. Y. B. Zel'Dovich and Y. P. Raizer, *Physics of Shock Waves and High-Temperature Hydrodynamic Phenomena* (Academic, 1966).
22. S. B. Wen, X. Mao, R. Greif, and R. E. Russo, "Laser ablation induced vapor plume expansion into a background gas. II. Experimental analysis," J. Appl. Phys. (Melville, NY, U. S.) **101**(2), 023115 (2007).
23. J. X. Wang, S. Q. Wang, L. Zhang, M. G. Su, D. X. Sun, Q. Min, W. G. Ma, W. B. Yin, and S. T. Jia, "Measurement and analysis of species distribution in laser-induced ablation plasma of an aluminum–magnesium alloy," Plasma Sci. Technol. **24**(3), 035005 (2022).